EasyChair Preprint

№ 9118

Fold-Change Detection (FCD) Synthetic Circuits

Rongying Huang and Ramez Daniel

October 24, 2022

Fold-Change Detection (FCD) Synthetic Circuits

Rongying Huang
Ramez Daniel*
Rongying.h@campus.technion.ac.il
Ramizda@bm.technion.ac.il

1 ABSTRACT

Cellular sensory systems often detect the input signal's relative change rather than its absolute value to eliminate the background noise and obtain more accurate signal detection. This property is known as fold-change detection (FCD), determined by the ratio between the ON and OFF states. Recent studies demonstrated that applying incoherent type-1 feedforward loops(I1-FFL) could lead to gene circuits that can compute FCD. In I1-FFL networks, the input signal is split into two pathways, where both control the output positively and negatively. The FCD could only be achieved when the strengths of the negative and positive pathways are optimized for specific values, limiting the implementation of I1-FFL in gene circuits. In this study, we present and analyze a new motif that coupled I1-FFL with a negative feedback loop for FCD. The simulation shows a significant improvement in the FCD performance and robustness with a wider-range input response.

Keywords: Synthetic biology, Fold Change Detection, In-silico design

2 INTRODUCTION

Fold Change Detection (FCD)

Synthetic biology has enabled the design of engineered genetic circuits to build robust biosensors for diverse applications [1]. These biosensors include synthetic genetic circuits in bacterial cells, which can apply for environmental toxic and pathogenic contaminants monitoring [2], [3], and disease diagnosis [4]. Particularly for these applications, the variation of input signals scale to the background (basal level) signal, resulting from the dynamic change of the environment, providing an opportunity for early-stage detection. Therefore, in many sensory systems, there is a dire need to measure FCD (see Figure 1), which describes a dynamics system determined by the relative change in the input signal instead of detecting the absolute signal's change. Furthermore, FCD circuits are also useful for achieving a perfect adaption when a disturbance is present [5].

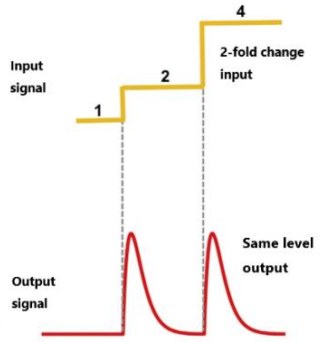

Figure 1 Fold-change detection (FCD) systems have an identical dynamical response to signals with the same fold-change.

Many biological behaviors including chemotaxis, vision, hearing, smell even psychological senses work in terms of FCD [6], [7]. In some biological systems, it shows evidence that the FCD is sharing a recurring gene regulatory network—the incoherent type-1 feedforward loop(I1-FFL) (Figure 2) [5]. The feedforward loop is 'incoherent' when an input signal X is split into two pathways, and it controls the output Z positively and negatively. Based on Figure 2, we can rewrite the Michaelis-Menten equation shown in Equation (1) where g=0.

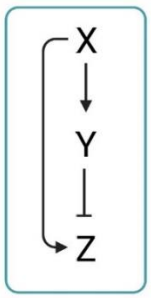

I1-FFL

Figure 2 A schematic diagram of the I1-FFL motif. An input signal X is split into two pathways, and it controls the output Z positively and negatively.

$$\begin{cases} \dfrac{dX}{dt} = -\dfrac{X}{\tau_X(1+g\cdot Y)} \\ \dfrac{dY}{dt} = \alpha_1 \dfrac{X}{K_X+X} - \beta_1 Y \\ \dfrac{dZ}{dt} = \alpha_2 \dfrac{1}{1+Y/K_Y}\cdot\dfrac{X}{K_X+X} - \beta_2 Z \end{cases} \quad (1) \xrightarrow{X\ll K_X, Y\gg K_Y} \begin{cases} \dfrac{dX}{dt} = -\dfrac{X}{\tau_X(1+g\cdot Y)} \\ \dfrac{dY}{dt} = \alpha_1' X - \beta_1' Y \\ \dfrac{dZ}{dt} = \alpha_2' \dfrac{X}{Y} - \beta_2' Z \end{cases} \quad (2)$$

Equation (1-2). In gene circuits, X and Y represent activator and repressor expression levels, respectively. α_1, α_2 are the production rate, and β_1, β_2 are represent the degradation rate of X, Y separately. K_X represents the dissociation constant of binding X to the appropriate DNA site in a specific promoter, and K_Y represents the dissociation constant of binding Y to the appropriate DNA site in the same specific promoter. $1/\tau_X$ is represent the degradation rate of input X. g indicates the intensity of the negative feedback from Y inhibits the production of X. If $g = 0$, the equation describes the I1-FFL. The I1-FFL circuit can compute FCD only when $X \ll K_X, Y \gg K_Y$, where the function can simplify as equation2. Here, we redefined the α_1', α_2' as the production rate, β_1', β_2' as the degradation rate for X, Y separately.

However, due to constraints on K_X and K_Y , the I1-FFL failed to sense the relative change when the input is very weak signals which are on the threshold of detection or very strong signals that saturate the receptors (see Figure 3). Therefore, the demand for the FCD circuit with an extended response range should have been uplifted. Because a negative feedback loop (NF) is a common motif who able to increase the time resolution of response and show pulses [5], we coupled I1-FFL with an additional negative feedback loop (NF) from Y inhibits the production of X (see Figure 4), to widen the detection range of the input signal as well as improved robustness and performance of the output signal. In such a case, based on Figure 4, the Michaelis-Menten equation for the I1-FFL-NF circuit could be rewritten as Equation (1) where g represents the intensity of the negative feedback to the input signal X.

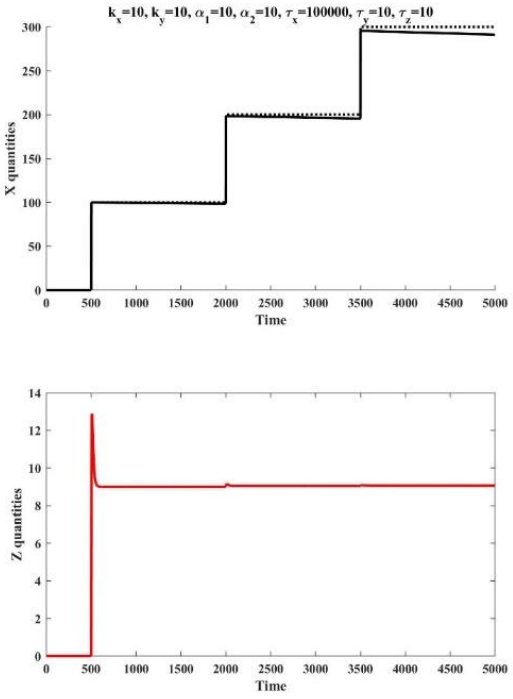

Figure 3 Simulation results of I1-FFL without NF where input X=100,200,300 at time=500,2000,3500 separately. And the parameter values were chosen as $k_x = 10, k_y = 10, \alpha_1 = 10, \alpha_2 = 10, \tau_x = 100000, \tau_y = 10, \tau_z = 10$ The black dashed curve represents the input signal X. the black curve represents the internal X concentration. The red curve Z shows the output signal.

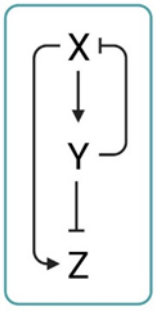

I1-FFL+NF

Figure 2 A schematic diagram of the I1-FFL-NF motif. Negative feedback occurs when Y inhibits the production of X.

***In-silico* design**

Numerous improvements in genetic circuit assembling have been made based on the computer-aided design which enables the quick exploration and testing of designs in-silico[8]. In addition, the in-silico design also

minimizes the need for expensive and laborious physical assembly and experimentation. To evaluate and optimize our design I1-FFL-NF circuit we stimulate both the I1-FFL and I1-FFL-NF gene regulatory network. If $X \ll K_X, Y \gg K_Y$, equation 1 can rewrite as equation 2. Based on Equation 1, when $g = 0$ the model can be simplified as an I1-FFL circuit. It shows that the I1-FFL-NF ($g > 0$) circuit with much wider dynamic response range and improved performance/robustness compared with the original I1-FFL design (see Figure 3).

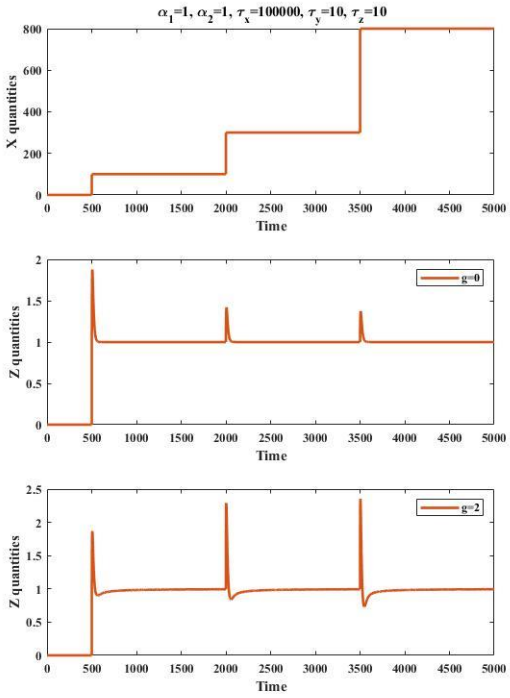

Figure 3 Based on equation 2, the simulation results illustrate the I1-FFL and I1-FFL-NF motif output signal under the same input signal. The parameter values were chosen as $\alpha_1 = 1, \alpha_2 = 1, \tau_x = 100000, \tau_y = 10, \tau_z = 10.$

Our I1-FFL-NF design shows a significant dependence on the parameters g of negative feedback. In the mathematical model part, we showed that FCD can only be realized when the binding of X to its target promoters is weak, and the binding of the repressor Y is strong ($X \ll K_X, Y \gg K_Y$). If the parameters not in such condition, the circuit fails to act as FCD shown as Figure 3 red curve and Figure 4 blue curve where the NF part is neglectable. While the NF part is getting stronger (Figure 4 red curve $g = 5$), the FCD can be achieved. And the I1-FFL-NF can show the exact adaptation (Figure 4 green curve) in high-intensity negative feedback ($g = 1000$). By tuning the intensity of the (parameter g) negative feedback, the design circuits can perform in a wider-dynamic-range input response for diverse application situations. Figure 5 shows the normalized Z value according to different negative strengths (g value). When the normalized Z value equals zero, the genetic circuit shows the exact adaptation. This g parameter can optimize experimental planning.

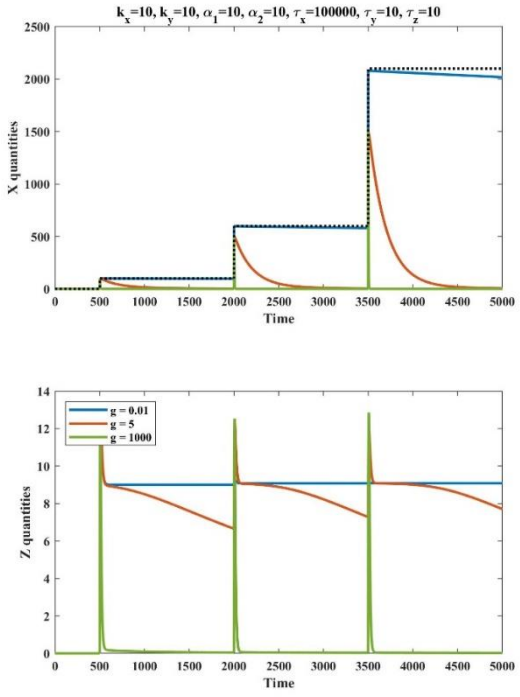

Figure 4 Simulation results of I1-FFL-NF with the different level intensity(g) of the negative feedback. X=100,500,1500 at time= 500,2000,3500 separately. In the upper figure, the curve shows the internal signal of the X, besides the black dashed curve, which represents the external input signal X. The lower figure shows the output Z signal based on different g values. $g = 0.01,5,1000$ *corresponding to blue, red, and green curves. g represents the strength of the NF shown in equation 1. The parameter values were chosen as* $k_x = 10, k_y = 10, \alpha_1 = 10, \alpha_2 = 10, \tau_x = 100000, \tau_y = 10, \tau_z = 10$

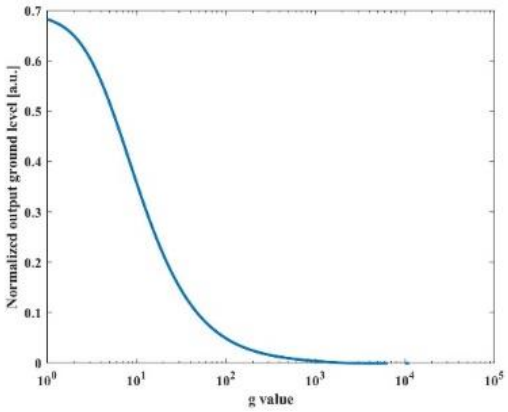

Figure 5 Following the upper case, the normalized Z value according to different strengths of negative feedback (g value). When the $g \cong 1e3$, the output signal Z shows the exact adaptation.

Bibliography

[1] A. S. Khalil and J. J. Collins, "Synthetic biology: Applications come of age," *Nat. Rev. Genet.*, vol. 11, no. 5, pp. 367–379, 2010, DOI: 10.1038/nrg2775.

[2] X. Wan, F. Volpetti, E. Petrova, C. French, S. J. Maerkl, and B. Wang, "Cascaded amplifying circuits enable ultrasensitive cellular sensors for toxic metals," *Nat. Chem. Biol.*, vol. 15, no. 5, pp. 540–548, 2019, DOI: 10.1038/s41589-019-0244-3.

[3] P. Litovco, N. Barger, X. Li, and R. Daniel, "Topologies of synthetic gene circuit for optimal fold change activation," *Nucleic Acids Res.*, vol. 49, no. 9, pp. 5393–5406, 2021, DOI: 10.1093/nar/gkab253.

[4] N. Barger, I. Oren, X. Li, M. Habib, and R. Daniel, "A Whole-Cell Bacterial Biosensor for Blood Markers Detection in Urine," *ACS Synth. Biol.*, vol. 10, no. 5, pp. 1132–1142, 2021, DOI: 10.1021/acssynbio.0c00640.

[5] U. Alon, *An introduction to systems biology*, vol. 62, no. 6. 2020.

[6] Y. Hart, H. Goldberg, E. Striem-Amit, A. E. Mayo, L. Noy, and U. Alon, "Creative exploration as a scale-invariant search on a meaning landscape," *Nat. Commun.*, vol. 9, no. 1, pp. 1–11, 2018, doi: 10.1038/s41467-018-07715-8.

[7] M. Adler and U. Alon, "Fold-change detection in biological systems," *Curr. Opin. Syst. Biol.*, vol. 8, pp. 81–89, 2018, doi: 10.1016/j.coisb.2017.12.005.

[8] T. S. Jones, S. M. D. Oliveira, C. J. Myers, C. A. Voigt, and D. Densmore, "Genetic circuit design automation with Cello 2.0," *Nat. Protoc.*, vol. 17, no. 4, pp. 1097–1113, 2022, doi: 10.1038/s41596-021-00675-2.